

Exact Floquet Quantum Many-Body Scars under Rydberg Blockade

Kaoru Mizuta,^{1,*} Kazuaki Takasan,² and Norio Kawakami¹

¹*Department of Physics, Kyoto University, Kyoto 606-8502, Japan*

²*Department of Physics, University of California, Berkeley, California 94720, USA*

(Dated: April 21, 2022)

Quantum many-body scars have attracted much interest as a violation of the eigenstate thermalization hypothesis (ETH) due to recent experimental observation in Rydberg atoms and related theoretical studies. In this paper, we construct a model hosting exact Floquet quantum many-body scars, which violate the Floquet version of ETH (Floquet-ETH). We consider two uniformly-driven static Hamiltonians prohibiting neighboring up spins (Rydberg blockade) like the PXP model, and construct a binary drive composed of them. We show that there exists a four-dimensional subspace which completely avoids thermalization to infinite temperature and that any other states, including some special scar states reported in the static PXP model, are vulnerable to heating and relax to infinite temperature. We also construct a more generalized periodic drive composed of time-dependent PXP-type Hamiltonians showing exact Floquet quantum many-body scars and discuss possible experimental realization of the model in Rydberg atoms.

I. INTRODUCTION

Thermalization in closed quantum systems has been vigorously studied to understand the relationship between quantum physics and statistical physics. With the recent progress in numerical and experimental studies [1–4], generic nonintegrable systems have been believed to satisfy so-called *eigenstate thermalization hypothesis* (ETH). ETH dictates that all the eigenstates cannot be distinguished from thermal equilibrium states as long as only macroscopic observables are considered. Since ETH is a sufficient condition for thermalization to take place, ETH is believed to be a key to understand thermalization.

However, with the development of Rydberg atoms [4], it has been revealed that there exists a violation of ETH called *quantum many-body scars* [5]. To be precise, there are several non-thermal eigenstates, which are eigenstates distinguishable from thermal equilibrium states (called exact scar eigenstates), while other states out of their subspace experience thermalization as with usual nonintegrable models. The PXP model, a typical model showing scars, has been realized on Rydberg atoms where adjacent atoms in Rydberg states are prohibited (Rydberg blockade) [6–9]. A non-thermalizing oscillation of domain wall density, which seems to be related to exact scar eigenstates [10], has been observed.

In contrast, in periodically driven (Floquet) cases, non-integrable systems are believed to satisfy the Floquet version of ETH (Floquet-ETH), which says that all the eigenstates of the time evolution operator for one period cannot be distinguished from a trivial infinite temperature state [11, 12]. This is a sufficient condition for any initial state to be thermalized to infinite temperature, which can be interpreted as a consequence from the absence of energy conservation. While many-body

physics causes various attractive phenomena in static systems, interacting Floquet systems often become trivial due to Floquet-ETH in the thermodynamic limit, except for a few examples such as Floquet many-body localization [13, 14] and Floquet time crystals [15–21]. Thus, quantum many-body scars in Floquet systems (Floquet quantum many-body scars) are also of great interest as a violation of Floquet-ETH.

Some recent studies have tackled the realization of Floquet quantum many-body scars [22–24]. The former references [22, 23] consider a system dominated by random unitary matrices preserving charges and dipole moments, and numerically (Ref. [22]) and analytically (Ref. [23]) show the existence of states immune to thermalization. The latter one [24] rigorously constructs Floquet quantum many-body scars realized by quasienergy-degeneracy modulo 2π (Floquet-intrinsic scars). Here, we demonstrate a new systematic construction of exact Floquet quantum many-body scars realized by a binary drive composed of uniformly-driven PXP-type static models. In our construction, the instantaneous Hamiltonians share a subspace immune to thermalization, though they have different non-thermal scar eigenstates. Using these properties, we can realize exact Floquet quantum many-body scars showing persistent dynamics both stroboscopically and microscopically without fine-tuning of the switching time. This also enables us to construct a generic periodic drive hosting exact Floquet quantum many-body scars. These results will shed a new light on understanding of nonequilibrium dynamics in Floquet systems.

II. MODELS AND OUTLINE

First, we identify the protocol of driving and show the outline of this paper. Floquet systems are described by a time-periodic Hamiltonian $H(t)$ which satisfies $H(t) = H(t + T)$ (T : period). Here, we focus on a binary drive

* mizuta.kaoru.65u@st.kyoto-u.ac.jp

as the simplest protocol, described by

$$H(t) = \begin{cases} H_1 & 0 \leq t < T_1 \\ H_2 & T_1 \leq t < T_1 + T_2 = T, \end{cases} \quad (1)$$

and then the Floquet operator U_f (the time evolution operator for one period T) is given by

$$U_f = e^{-iH_2T_2}e^{-iH_1T_1}. \quad (2)$$

What distinguishes Floquet systems from static systems is the non-commutative property of Hamiltonians at different time, and hence we assume

$$[H_1, H_2] \neq 0. \quad (3)$$

To construct Floquet quantum many-body scars, we make use of two different static Hamiltonians H_1 and H_2 hosting quantum many-body scars. With choosing proper uniform PXP-type Hamiltonians, defined on a Hilbert space prohibiting adjacent up spins (Rydberg blockade), we rigorously show the existence of a four-dimensional subspace immune to relaxation to infinite temperature.

Following the above strategy, this paper is organized as follows. In Section III, we introduce two static models hosting quantum many-body scars. One of them is a well-known model called the PXP model. We construct the PY₄P model as another model inequivalent to the PXP model. In Section IV, we construct a binary drive which shows Floquet quantum many-body scars using these static models, and numerically examine its nonintegrability to demonstrate that it can be a nontrivial example for the violation of Floquet-ETH. Then, we rigorously show the existence of an embedded subspace, which is a subspace completely immune to thermalization. We also demonstrate the real-time dynamics and show thermalization dependent on whether the initial states belong to the embedded subspace (Section V). Finally, we discuss generalization of our binary drive to a generic time-periodic drive (Section VI) and end up with discussing a possible experimental realization in Rydberg atoms and concluding this paper (Section VII).

III. STATIC MODELS

A. PXP model and PY₄P model

In this section, we introduce the PXP model as a typical static model showing scars, and construct another model called the PY₄P model with its analogy. Throughout the paper, we consider a one-dimensional Ising chain under open boundary conditions (OBC). Assume that the number of the sites L is a multiple of four. We consider a Hilbert space prohibiting states which include neighboring up spins, and then the dimension of the Hilbert space \mathcal{D}_L is given by $\mathcal{D}_L = F_{L+2}$ (F_n : the Fibonacci sequence) [25]. The PXP model under OBC is

described by the following Hamiltonian [4, 6]:

$$H_X = \sum_{i=2}^{L-1} P_{i-1} X_i P_{i+1} + X_1 P_2 + P_{L-1} X_L, \quad (4)$$

$$P_i = (1 - Z_i)/2. \quad (5)$$

Here, we denote Pauli operators on the i -th site by I_i, X_i, Y_i and Z_i . P_i represents the projection to a down spin state on the i -th site. Such a Hamiltonian on the constrained Hilbert space is realizable in Rydberg atoms by quite strong repulsive interactions between adjacent atoms in Rydberg states [4]. The PXP model is known to violate ETH since the following four eigenstates $|\Gamma_{\alpha\beta}^x\rangle$ ($\alpha, \beta = 1, 2$) are not thermal [10]:

$$|\Gamma_{\alpha\beta}^x\rangle = \sum_{\vec{\sigma}} \vec{u}_{\alpha}^{\dagger} B^{\sigma_1} C^{\sigma_2} \dots B^{\sigma_{L-1}} C^{\sigma_L} \vec{u}_{\beta} |\vec{\sigma}\rangle \quad (6)$$

$$B^{\uparrow} = \sqrt{2} \begin{pmatrix} 0 & 0 & 0 \\ 1 & 0 & 1 \end{pmatrix}, \quad B^{\downarrow} = \begin{pmatrix} 1 & 0 & 0 \\ 0 & 1 & 0 \end{pmatrix}, \quad (7)$$

$$C^{\uparrow} = \sqrt{2} \begin{pmatrix} 1 & 0 \\ 0 & 0 \\ -1 & 0 \end{pmatrix}, \quad C^{\downarrow} = \begin{pmatrix} 0 & -1 \\ 1 & 0 \\ 0 & 0 \end{pmatrix}, \quad (8)$$

$$\vec{u}_1 = \frac{1}{\sqrt{2}} \begin{pmatrix} 1 \\ 1 \end{pmatrix}, \quad \vec{u}_2 = \frac{1}{\sqrt{2}} \begin{pmatrix} 1 \\ -1 \end{pmatrix}, \quad (9)$$

and they satisfy

$$\begin{aligned} H_X |\Gamma_{11}^x\rangle &= 0, & H_X |\Gamma_{12}^x\rangle &= \sqrt{2} |\Gamma_{12}^x\rangle, \\ H_X |\Gamma_{22}^x\rangle &= 0, & H_X |\Gamma_{21}^x\rangle &= -\sqrt{2} |\Gamma_{21}^x\rangle. \end{aligned} \quad (10)$$

For convenience, we define the b -th block by a pair of neighboring spins at the $(2b-1)$ -th site and $2b$ -th site. Then, each block can take three states $\uparrow\downarrow$, $\downarrow\downarrow$, and $\downarrow\uparrow$, which we denote as $s = L, O, R$ respectively. Then, the states $|\Gamma_{\alpha\beta}^x\rangle$ are rewritten as follows:

$$|\Gamma_{\alpha\beta}^x\rangle = \sum_{\vec{s}} \vec{u}_{\alpha}^{\dagger} A^{s_1} \dots A^{s_{L_b}} \vec{u}_{\beta} |\vec{s}\rangle, \quad (11)$$

$$\begin{aligned} A^L &= \begin{pmatrix} 0 & 0 \\ 0 & -\sqrt{2} \end{pmatrix}, & A^O &= \begin{pmatrix} 0 & -1 \\ 1 & 0 \end{pmatrix}, \\ A^R &= \begin{pmatrix} \sqrt{2} & 0 \\ 0 & 0 \end{pmatrix}, \end{aligned} \quad (12)$$

where the number of the blocks is $L_b = L/2$. The derivation of these relations is given in Ref. [10].

Next, we construct another static model, the PY₄P model, described by

$$H_Y = \sum_{i=2}^{L-1} (-c_i) P_{i-1} Y_i P_{i+1} - Y_1 P_2 - P_{L-1} Y_L, \quad (13)$$

$$c_i = \sqrt{2} \cos\left(\frac{i\pi}{2} - \frac{\pi}{4}\right), \quad (14)$$

which possesses quadruple lattice-periodicity. We define four states $|\Gamma_{\alpha\beta}^y\rangle$ by

$$|\Gamma_{\alpha\beta}^y\rangle = \sum_{\vec{s}} \vec{v}_\alpha^\dagger A^{s_1} \dots A^{s_{L_b}} \vec{v}_\beta |\vec{s}\rangle \quad (15)$$

$$\vec{v}_1 = \frac{1}{\sqrt{2}} \begin{pmatrix} 1 \\ i \end{pmatrix}, \quad \vec{v}_2 = \frac{1}{\sqrt{2}} \begin{pmatrix} 1 \\ -i \end{pmatrix}. \quad (16)$$

In a similar way to the derivation of the PXP model, we can show that these four states are exact scar eigenstates of the PY₄P model as follows:

$$\begin{aligned} H_Y |\Gamma_{11}^y\rangle &= 0, & H_Y |\Gamma_{12}^y\rangle &= \sqrt{2} |\Gamma_{12}^y\rangle, \\ H_Y |\Gamma_{22}^y\rangle &= 0, & H_Y |\Gamma_{21}^y\rangle &= -\sqrt{2} |\Gamma_{21}^y\rangle. \end{aligned} \quad (17)$$

B. Exact Scar eigenstates of PY₄P model

In this section, we derive Eq. (17). This calculation is necessary to obtain the physical interpretation of the absence of thermalization in our periodically-driven model (Section IV) and generalize our binary drive to generic time-periodic drives (Section VI). This part can be skipped if the reader is only interested in the existence of exact Floquet quantum many-body scar eigenstates and other thermal behaviors in the model.

Proof.— We consider the PY₄P Hamiltonian H_Y based on blocks of neighboring two spins. We denote a state of the b -th block composed of the $(2b-1)$ -th and $2b$ -th spins by $|O\rangle_b = |\downarrow\downarrow\rangle_{2b-1,2b}$, $|L\rangle_b = |\uparrow\downarrow\rangle_{2b-1,2b}$, and $|R\rangle_b = |\downarrow\uparrow\rangle_{2b-1,2b}$. Let us focus on the term $h_{b,b+1}^y$, which is nontrivially acting on the b -th and $(b+1)$ -th blocks. Then, for b in the bulk ($2 \leq b \leq L_b - 1$),

$$\begin{aligned} h_{b,b+1}^y &= (-1)^{b-1} (P_{2b-1} Y_{2b} P_{2b+1} + P_{2b} Y_{2b+1} P_{2b+2}) \\ &= i(-1)^{b-1} (|O\rangle_b \langle R| - |R\rangle_b \langle O|)_b (I - |L\rangle_b \langle L|)_{b+1} \\ &\quad + i(-1)^{b-1} (I - |R\rangle_b \langle R|)_b (|O\rangle_b \langle L| - |L\rangle_b \langle O|)_{b+1} \\ &\equiv h_{b,b+1}^{y,(2)} + h_{b,b+1}^{y,(1)}, \end{aligned} \quad (18)$$

$$h_{b,b+1}^{y,(2)} = i(-1)^{b-1} \{ |RL\rangle_b (\langle OL| + \langle RO|) - \text{h.c.} \}_{b,b+1}, \quad (19)$$

$$\begin{aligned} h_{b,b+1}^{y,(1)} &= i(-1)^{b-1} (|O\rangle_b \langle R| - |R\rangle_b \langle O|)_b \\ &\quad + i(-1)^{b-1} (|O\rangle_b \langle L| - |L\rangle_b \langle O|)_{b+1} \end{aligned} \quad (20)$$

are obtained. The boundary terms of H_Y are given by

$$-Y_1 P_2 = i(|L\rangle_1 \langle O| - |O\rangle_1 \langle L|)_1, \quad (21)$$

$$-P_{L-1} Y_L = -i(|O\rangle_{L-1} \langle R| - |R\rangle_{L-1} \langle O|)_{L-1}. \quad (22)$$

Using the properties $A^R A^L = O$ and $A^O A^L + A^R A^O = O$ results in

$$h_{b,b+1}^{y,(2)} |\Gamma_{\alpha\beta}^y\rangle = 0, \quad b = 2, 3, \dots, L_b - 1. \quad (23)$$

Thus, only the single-body terms have a nonzero contribution:

$$H_Y |\Gamma_{\alpha\beta}^y\rangle = \sum_{b=1}^{L_b} h_b^{y,(1)} |\Gamma_{\alpha\beta}^y\rangle, \quad (24)$$

$$h_b^{y,(1)} = (-1)^{b-1} i(|O\rangle_b \langle R| + |L\rangle_b \langle O| - \text{h.c.})_b. \quad (25)$$

To calculate this, we consider superblocks corresponding to pairs of neighboring blocks. Here, we define a u -th superblock by a pair of $(2u-1)$ -th and $2u$ -th blocks. Each superblock has seven degrees of freedom $t_u = (s_{(2u-1)}, s_{2u}) = OO, LL, RR, OL, OR, LO, RO$, while RL and LR are not included in $|\Gamma_{\alpha\beta}^y\rangle$ because of $A^R A^L = A^L A^R = 0$. Then, the states $|\Gamma_{\alpha\beta}^y\rangle$ are rewritten in the following form,

$$|\Gamma_{\alpha\beta}^y\rangle = \sum_{\vec{t}} \vec{v}_\alpha^\dagger \tilde{A}^{t_1} \dots \tilde{A}^{t_{L_u}} \vec{v}_\beta |\vec{t}\rangle, \quad (26)$$

$$\vec{t} = (t_1, \dots, t_{L_u}), \quad L_u = L_b/2 = L/4. \quad (27)$$

The matrices \tilde{A}^t are given by

$$\begin{aligned} \tilde{A}^t &= A^s A^r, \quad t = (s, r), \\ \tilde{A}^{OO} &= -\sigma^0, \quad \tilde{A}^{LL} = \sigma^0 - \sigma^z, \quad \tilde{A}^{RR} = \sigma^0 + \sigma^z, \\ \tilde{A}^{OL} &= -\tilde{A}^{RO} = (\sigma^x + i\sigma^y)/\sqrt{2}, \\ \tilde{A}^{OR} &= -\tilde{A}^{LO} = (\sigma^x - i\sigma^y)/\sqrt{2}. \end{aligned} \quad (28)$$

The action of $h_{2u-1}^{y,(1)} + h_{2u}^{y,(1)}$ is described by

$$(h_{2u-1}^{y,(1)} + h_{2u}^{y,(1)}) |\Gamma_{\alpha\beta}^y\rangle = \sum_{\vec{t}} \vec{v}_\alpha^\dagger \tilde{A}^{t_1} \dots \tilde{F}^{t_u} \dots \tilde{A}^{t_{L_u}} \vec{v}_\beta |\vec{t}\rangle, \quad (29)$$

$$\tilde{F}^{(s,r)} = \left[\sum_{s'} (h_{2u-1}^{y,(1)})_{ss'} A^{s'} \right] A^r + A^s \left[\sum_{s'} (h_{2u}^{y,(1)})_{rr'} A^{r'} \right], \quad (30)$$

$$\begin{aligned} \tilde{F}^{OO} &= O, \quad \tilde{F}^{LL} = -\tilde{F}^{RR} = -\sqrt{2}i\sigma^x, \\ \tilde{F}^{OL} &= \tilde{F}^{OR} = -\tilde{F}^{LO} = -\tilde{F}^{RO} = -i\sigma^z. \end{aligned} \quad (31)$$

When we define $Y = \sigma^y/\sqrt{2}$, the matrices \tilde{A}^t and \tilde{F}^t are related as follows:

$$\tilde{F}^t = Y \tilde{A}^t - \tilde{A}^t Y, \quad t = OO, LL, RR, OL, OR, LO, RO. \quad (32)$$

Finally, we obtain

$$\begin{aligned} H_Y |\Gamma_{\alpha\beta}^y\rangle &= \sum_{b=1}^{L_b} h_b^{y,(1)} |\Gamma_{\alpha\beta}^y\rangle \\ &= \sum_{u, \vec{t}} \vec{v}_\alpha^\dagger \tilde{A}^{t_1} \dots (Y \tilde{A}^{t_u} - \tilde{A}^{t_u} Y) \dots \tilde{A}^{t_{L_u}} \vec{v}_\beta |\vec{t}\rangle \\ &= \sum_{\vec{t}} \vec{v}_\alpha^\dagger Y \tilde{A}^{t_1} \dots \tilde{A}^{t_{L_u}} \vec{v}_\beta |\vec{t}\rangle \\ &\quad - \sum_{\vec{t}} \vec{v}_\alpha^\dagger \tilde{A}^{t_1} \dots \tilde{A}^{t_{L_u}} Y \vec{v}_\beta |\vec{t}\rangle \\ &= \frac{1}{\sqrt{2}} \{ (-1)^{\alpha-1} - (-1)^{\beta-1} \} |\Gamma_{\alpha\beta}^y\rangle. \end{aligned} \quad (33)$$

In the last equality, we have used Eq. (16) indicating that $\vec{v}_{1,2}$ are eigenvectors of Y . Thus, we obtain Eqs. (17). \square

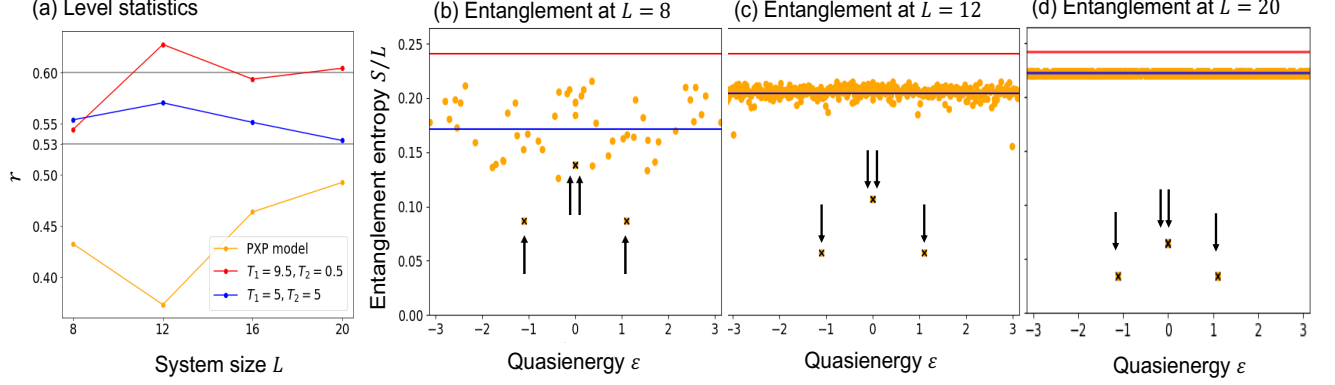


FIG. 1. (a) Level statistics of the PXP model (the yellow line) and the periodically-driven model (the red and blue lines). In the Floquet case, it rapidly approaches a value close to 0.6 ($T_1 = 9.5, T_2 = 0.5$) or 0.53 ($T_1 = T_2 = 5$, with time-reversal symmetry) as the system size grows. Both results imply the nonintegrability of the driven model. (b)-(d): Entanglement entropy per length for each Floquet eigenstate of a different system size (b) $L = 8$, (c) $L = 12$, and (d) $L = 20$. We use $T_1 = 9.5$ and $T_2 = 0.5$ as the parameters. The blue (lower solid) lines, representing the mean values of entanglement entropy, approach the red (upper solid) lines which denote the one at infinite temperature as the system size increases. The four marked states designated by the arrows (two points are degenerated at $\varepsilon = 0$) remain low-entangled since they are exact scar eigenstates of the periodically-driven model within the embedded subspace \mathcal{S} .

IV. FLOQUET QUANTUM MANY-BODY SCARS

In this section, we construct a binary drive showing Floquet quantum many-body scars. To confirm that our model becomes a nontrivial example violating Floquet-ETH, we numerically demonstrate nonintegrability of our model, and rigorously proves the existence of exact Floquet scar eigenstates, which are distinguishable from infinite temperature states.

A. Model

Assume that the system is a one-dimensional Ising chain where pairs of neighboring up spins are prohibited. Then, we consider a binary drive composed of the static Hamiltonians in the previous section:

$$H(t) = \begin{cases} H_X & 0 \leq t < T_1 \\ H_Y & T_1 \leq t < T_1 + T_2 = T, \end{cases} \quad (35)$$

and then its Floquet operator is written by

$$U_f = e^{-iH_Y T_2} e^{-iH_X T_1}. \quad (36)$$

Here, for Floquet quantum many-body scars to take place, T_1 and T_2 are arbitrary except for the case when either one of them is zero (there is no need for fine-tuning of them).

We note the symmetries underlying in this model. First, it possesses an inversion symmetry I which maps

each i -th site to $(L - i + 1)$ -th site, and the Floquet operator U_f is invariant under the inversion. Second, a nonlocal chiral symmetry \mathcal{C} , designated by

$$\mathcal{C} U_f \mathcal{C}^\dagger = U_f^\dagger, \quad \mathcal{C} = \left(\prod_i Z_i \right) e^{iH_Y T_2}, \quad (37)$$

is also respected. This chiral symmetry makes the spectrum of quasienergy $\{\varepsilon\}$ (the eigenvalues of $-i \log U_f$) symmetric to $\varepsilon = 0$. In addition, if $T_1 = T_2$ is satisfied, the model also respects a time-reversal symmetry (TRS), described by

$$U_Z U_f^* U_Z^\dagger = U_f^\dagger, \quad U_Z = \exp \left(-i \frac{\pi}{4} \sum_i c_i Z_i \right). \quad (38)$$

B. Nonintegrability

To confirm that the model can be a nontrivial example of violation of Floquet-ETH, we begin with analyzing nonintegrability of the model. Considering the nonintegrability of the PXP model, that of the PY₄P model [6, 26], and the noncommutability $[H_X, H_Y] \neq 0$, the model is also expected to be nonintegrable. Here, we demonstrate this by calculating level statistics. Using the n -th quasienergy ε_n (replaced by eigenenergy E_n in static cases) and its gap $\Delta_n = \varepsilon_{n+1} - \varepsilon_n$, let us define the level spacing ratio r_n by $r_n = \min(\Delta_n/\Delta_{n+1}, \Delta_{n+1}/\Delta_n)$ and denote their spectrally averaged value by $r \equiv \langle r_n \rangle$. When the model is nonintegrable with the increasing system size, r approaches a Gaussian orthogonal ensemble

(GOE) value close to 0.53 if it is time-reversal symmetric, or approaches a Gaussian unitary ensemble (GUE) value close to 0.6 otherwise [26–28]. On the other hand, in integrable systems, it approaches a value close to 0.39, that of Poisson statistics.

Figure 1 (a) shows the numerical result for r calculated by exact diagonalization (ED). Considering the inversion symmetry I , we limit the Hilbert space to the inversion-plus sector, the subspace whose eigenvalue of I is +1. The red upper solid line (blue middle solid line) represents the case of $T_1 = 9.5, T_2 = 0.5$ without TRS (that of $T_1 = T_2 = 5$ with TRS) respectively. In each case, r flows to a value close to 0.6 (a value close to 0.53) as the system size grows, and hence we can conclude the nonintegrability of the model.

We also demonstrate the nonintegrability in terms of entanglement entropy of each Floquet eigenstate. Entanglement entropy of a given state $|\psi\rangle$ is defined by

$$S[\psi] = -\text{Tr}_A[\rho_A \log \rho_A], \quad \rho_A = \text{Tr}_B |\psi\rangle \langle \psi|, \quad (39)$$

where the subsystems A (B) represents the left (right) half of the system respectively. A state $|\psi\rangle$ indistinguishable from the infinite temperature state is expected to possess entanglement entropy equal to that of infinite temperature S_∞ , and hence it obeys a volume law in the thermodynamic limit as follows [25]:

$$\lim_{L \rightarrow \infty} \frac{S_\infty}{L} = \frac{1}{2} \log \phi, \quad \phi = \frac{1 + \sqrt{5}}{2}. \quad (40)$$

Figure 1 (b)-(d) shows the numerical results at $T_1 = 9.5$ and $T_2 = 0.5$. The red lines are entanglement entropy per volume at infinite temperature, while the blue lines represent the averaged entanglement entropy per volume of all the Floquet eigenstates. As the system size L increases, Floquet eigenstates become featureless, with its entanglement entropy approaching the one at infinite temperature. On the other hand, there exist four anomalous low-entangled Floquet eigenstates designated by the four marked points in the figure. As discussed in the following section, these four states are nothing but exact Floquet scar eigenstates, which are distinguishable from the infinite temperature state. This result elucidates both the nonintegrability and the existence of nontrivial Floquet quantum many-body scars.

C. Exact Floquet Scar eigenstates

We rigorously show a violation of Floquet-ETH in our model. To be precise, we prove that there exist four exact Floquet scar eigenstates, which can be distinguished from infinite temperature states. We define \mathcal{S} by the four-dimensional subspace spanned by $\{|\Gamma_{\alpha\beta}^x\rangle\}_{\alpha,\beta=1,2}$. Within the subspace \mathcal{S} , thermalization does not take place under $\exp(-iH_X T_1)$ by its definition. On the other hand, using

Eqs. (11) and (15), we obtain

$$\begin{aligned} |\Gamma_{11}^y\rangle &= \frac{1}{2}(|\Gamma_{11}^x\rangle + i|\Gamma_{12}^x\rangle - i|\Gamma_{21}^x\rangle + |\Gamma_{22}^x\rangle), \\ |\Gamma_{12}^y\rangle &= \frac{1}{2}(i|\Gamma_{11}^x\rangle + |\Gamma_{12}^x\rangle + |\Gamma_{21}^x\rangle - i|\Gamma_{22}^x\rangle), \\ |\Gamma_{21}^y\rangle &= \frac{1}{2}(-i|\Gamma_{11}^x\rangle + |\Gamma_{12}^x\rangle + |\Gamma_{21}^x\rangle + i|\Gamma_{22}^x\rangle), \\ |\Gamma_{22}^y\rangle &= \frac{1}{2}(|\Gamma_{11}^x\rangle - i|\Gamma_{12}^x\rangle + i|\Gamma_{21}^x\rangle + |\Gamma_{22}^x\rangle). \end{aligned} \quad (41)$$

Since this transformation is invertible, the subspace \mathcal{S} is identical to the one spanned by $\{|\Gamma_{\alpha\beta}^y\rangle\}_{\alpha,\beta=1,2}$. Thus, thermalization does not take place in the subspace \mathcal{S} also under $\exp(-iH_Y T_2)$, and hence we can conclude the absence of thermalization in the subspace \mathcal{S} under the Floquet operator U_f . This can be understood also from local conserved quantities in the embedded subspace \mathcal{S} . From Eq. (23) and similar relations of the PXP model, the interaction terms of the Hamiltonian disappear within \mathcal{S} , and this results in the Floquet operator on \mathcal{S} as follows:

$$U_f|_{\mathcal{S}} = \prod_{b=1}^{L_b} \left(e^{-iT_2 h_b^{y,(1)}} e^{-iT_1 h_b^{x,(1)}} \right), \quad (42)$$

$$h_b^{x,(1)} = (|O\rangle \langle L| + |O\rangle \langle R| + \text{h.c.})_b. \quad (43)$$

Therefore, a set of local observables defined by $\{-i \log(\exp(-iT_2 h_b^{y,(1)}) \exp(-iT_1 h_b^{x,(1)}))\}_b$ composes a macroscopic number of local conserved quantities of the system, and this implies the absence of thermalization in \mathcal{S} .

The existence of the four-dimensional embedded subspace ensures the existence of four exact Floquet scar eigenstates. Two of them given by

$$\begin{aligned} |\Gamma_0\rangle &= |\Gamma_{11}^x\rangle + |\Gamma_{22}^x\rangle, \\ |\Gamma'_0\rangle &= \sin \frac{T_1}{\sqrt{2}} \cos \frac{T_2}{\sqrt{2}} (|\Gamma_{11}^x\rangle - |\Gamma_{22}^x\rangle) \\ &\quad + i \sin \frac{T_2}{\sqrt{2}} (e^{iT_1/\sqrt{2}} |\Gamma_{12}^x\rangle - e^{-iT_1/\sqrt{2}} |\Gamma_{21}^x\rangle), \end{aligned} \quad (44)$$

have quasienergy 0 and are invariant under the chiral symmetry operation \mathcal{C} modulo constant. The other two eigenstates are related to each other by \mathcal{C} and hence they have quasienergies with the opposite signs, though their analytical forms are too complicated to be shown here. Since \mathcal{C} becomes an onsite symmetry within \mathcal{S} due to Eqs. (23) and (37), they have the same entanglement entropy, while other pairs outside of \mathcal{S} do not. These four states appear in Fig. 1 (b)-(d) as the four marked low-entangled states. Since they are represented by matrix product states with at-most bond dimension 8, their entanglement entropy per length decays with $O(1/L)$, corresponding to the numerical result.

Finally, to confirm the violation of Floquet ETH, we examine whether Floquet eigenstates within the subspace \mathcal{S} can be distinguished from the infinite temperature

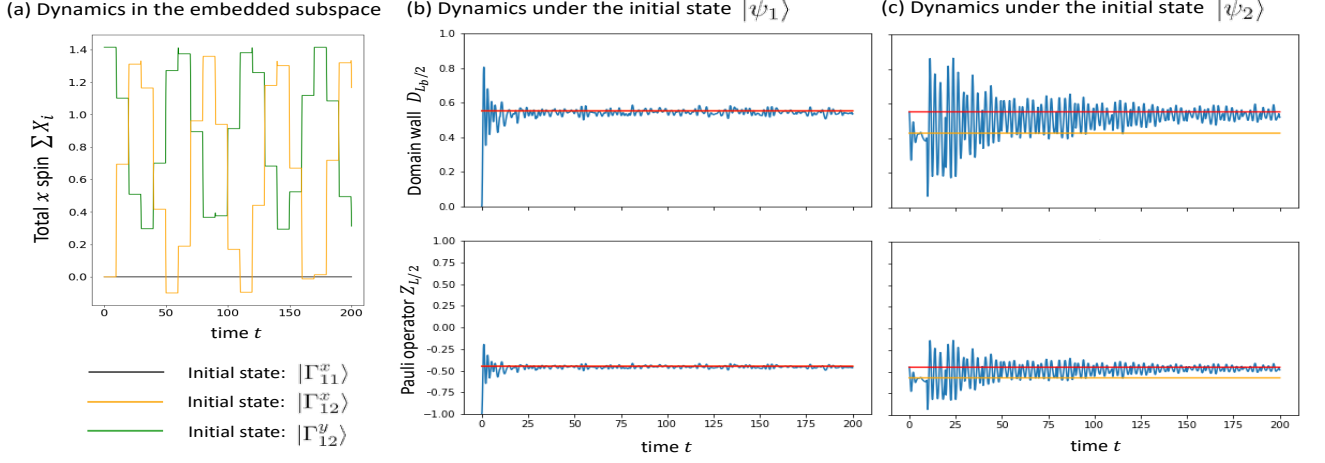


FIG. 2. (a) Real-time dynamics of total x spin $\sum_i X_i$ under the initial states within \mathcal{S} at $T_1 = 9.5, T_2 = 0.5$. The states $|\Gamma_{12}^x\rangle$ and $|\Gamma_{12}^y\rangle$ show a persistent oscillation. (b) Real-time dynamics under the initial state $|\psi_1\rangle$, which is at infinite temperature under H_X . The red lines represent the values at infinite temperature. (c) Real-time dynamics under the initial state $|\psi_2\rangle$, which is at finite temperature β_{eff} under H_X . The lower solid yellow lines represent the finite-temperature-equilibrium values under H_X [β_{eff} is obtained by numerically solving Eq. (50)]. The Floquet drive breaks such a feature of the initial state, and makes the observable approach the values at infinite temperature (the upper solid red lines).

state. Here, we focus on a domain wall density defined by

$$D_b \equiv \frac{1}{2}(I - Z_{2b-1}Z_{2b}). \quad (46)$$

Then, the expectation value of D_b is obtained as

$$\lim_{L_b \rightarrow \infty} \langle \psi | D_b | \psi \rangle = \frac{2}{3} \quad (47)$$

for any state $|\psi\rangle \in \mathcal{S}$, $\langle \psi | \psi \rangle = 1$ including the renormalized eigenstates of U_f within \mathcal{S} [See Appendix A1 C]. On the other hand, the expectation value of domain wall density at infinite temperature in the thermodynamic limit is $2/\sqrt{5}\phi = 0.542\dots \neq 2/3$ (ϕ : the golden ratio) under OBC [See Appendix A2 B]. Therefore, it can be concluded that the model Eq. (35) violates Floquet-ETH.

V. REAL-TIME DYNAMICS

We discuss the real-time dynamics in and out of the embedded subspace \mathcal{S} , which possibly leads to experimental detection of Floquet quantum many-body scars.

First, let us consider the real-time dynamics within the embedded subspace \mathcal{S} . We define renormalized scar eigenstates by $|\tilde{\Gamma}_{\alpha\beta}^x\rangle \equiv |\Gamma_{\alpha\beta}^x\rangle / \|\Gamma_{\alpha\beta}^x\rangle\|$, and then $\{|\tilde{\Gamma}_{11}^x\rangle, |\tilde{\Gamma}_{12}^x\rangle, |\tilde{\Gamma}_{21}^x\rangle, |\tilde{\Gamma}_{22}^x\rangle\}$ composes an orthonormal basis of \mathcal{S} in the thermodynamic limit while $|\Gamma_{11}^x\rangle$ is not orthogonal to $|\Gamma_{22}^x\rangle$ [29]. With this basis, the Floquet

operator $U_f|_{\mathcal{S}}$ is represented by

$$U_f|_{\mathcal{S}} = \begin{pmatrix} p & qr & qr^* & 1-p \\ -q & pr & -(1-p)r^* & q \\ -q & -(1-p)r & pr^* & q \\ 1-p & -qr & -qr^* & p \end{pmatrix}, \quad (48)$$

$$p = \frac{1 + \cos \sqrt{2}T_2}{2}, \quad q = \frac{\sin \sqrt{2}T_2}{2}, \quad r = e^{-i\sqrt{2}T_1}, \quad (49)$$

and stroboscopic dynamics of any observable is determined by its matrix representation. For example, the total magnetization in the x direction, $\lim_{L \rightarrow \infty} \sum_i X_i$, is given by $\text{diag}(0, \sqrt{2}, -\sqrt{2}, 0)$ and shows a persistent oscillation in general, while the local Pauli operator Z_i and the domain wall density D_b remain constant since they are proportional to identity in \mathcal{S} [29]. On the other hand, concerning the microscopic dynamics, generic initial states in \mathcal{S} , different from $|\Gamma_0\rangle$, show some persistent motion since $|\Gamma_0\rangle$ is the unique simultaneous eigenstate of H_X and H_Y in \mathcal{S} . We show typical real-time dynamics in Fig. 2 (a).

Next, we demonstrate the behavior outside of the embedded subspace \mathcal{S} . Following the nonintegrability of the model, generic initial states are expected to relax to infinite temperature, and we numerically confirm it by ED [See Fig. 2 (b), (c)]. We consider two different initial states $|\psi_1\rangle \equiv |\downarrow\downarrow\dots\rangle$ and $|\psi_2\rangle \equiv \mathcal{P}|\rightarrow\rangle^{\otimes L}/\sqrt{\mathcal{D}_L}$, where we define $|\rightarrow\rangle$ by $(|\uparrow\rangle - |\downarrow\rangle)/\sqrt{2}$ and denote the projection to the constrained Hilbert space prohibiting adjacent up spins as \mathcal{P} . They have an exponentially small overlap

with \mathcal{S} in terms of the system size, and $|\psi_1\rangle$ ($|\psi_2\rangle$) is an infinite-temperature state (a state with finite temperature β_{eff}) under the PXP Hamiltonian H_X because of $\langle\psi_1|H_X|\psi_1\rangle = 0$ ($\langle\psi_2|H_X|\psi_2\rangle = -2L/\sqrt{5}\phi$). Here, the temperature of a state $|\psi\rangle$ is determined by solving the energy conservation

$$\frac{\langle\psi|H_X|\psi\rangle}{\langle\psi|\psi\rangle} = \frac{\text{Tr}[H_X e^{-\beta H_X}]}{\text{Tr}[e^{-\beta H_X}]} \quad (50)$$

in terms of β . Figure 2 (b) and (c) show the dynamics at $T_1 = 9.5$ and $T_2 = 0.5$, which we choose so that pre-equilibration under an effective static Hamiltonian in the high-frequency regime can be avoided [30–33]. The model shows thermalization to infinite temperature regardless of initial states outside of the embedded subspace in contrast to the static PXP model and the PY₄P model, where the system relaxes to thermal states with a certain temperature depending on its initial states.

In the static PXP model, there also exist some special states such as $|\mathbb{Z}_2\rangle \equiv |\uparrow\downarrow\uparrow\downarrow\dots\rangle$ which show non-thermalizing behaviors of observables (e.g. domain wall density), though their overlap with the embedded subspace is small enough [4, 6, 8, 10]. We demonstrate the existence of such special states in the periodically-driven model in Appendix A3 [34]. The numerical result says that such a special state is thermalized to infinite temperature as well as other generic initial states out of the embedded subspace. In the static PXP model and the PY₄P model, three types of dynamics—complete absence of thermalization within the embedded subspace, seemingly non-thermalizing behavior of some special states, and thermalization of other generic states, are observed. By contrast, we conclude that the periodically-driven model only shows complete absence of thermalization to infinite temperature within the embedded subspace or thermalization of other generic states.

VI. GENERALIZATION

We generalize our binary drive to generic time-periodic drives. For this purpose, we first introduce another static model, the PZ₄P model defined by

$$H_Z = \sum_{i=2}^{L-1} c_i P_{i-1} Q_i P_{i+1} + Q_1 P_2 + P_{L-1} Q_L, \quad (51)$$

$$Q_i = I_i - P_i = (1 + Z_i)/2. \quad (52)$$

Then, the PZ₄P model possesses the following eigenstates:

$$\begin{aligned} H_Z |\Gamma_{11}^z\rangle &= 0, & H_Z |\Gamma_{12}^z\rangle &= \sqrt{2} |\Gamma_{12}^z\rangle, \\ H_Z |\Gamma_{22}^z\rangle &= 0, & H_Z |\Gamma_{21}^z\rangle &= -\sqrt{2} |\Gamma_{21}^z\rangle, \end{aligned} \quad (53)$$

where $\{|\Gamma_{\alpha\beta}^z\rangle\}$ is given by

$$|\Gamma_{\alpha\beta}^z\rangle = \sum_{\vec{\sigma}} \vec{w}_\alpha^\dagger A^{s_1} \dots A^{s_{L_b}} \vec{w}_\beta |\vec{s}\rangle, \quad (54)$$

$$\vec{w}_1 = \begin{pmatrix} 1 \\ 0 \end{pmatrix}, \quad \vec{w}_2 = \begin{pmatrix} 0 \\ 1 \end{pmatrix}. \quad (55)$$

This derivation is given in Appendix [29]. Since the Hamiltonian H_Z commutes with Z_i for every i , the PZ₄P model is integrable and does not host nontrivial phenomena by itself. However, by combining the PXP Hamiltonian and the PY₄P Hamiltonian, we can construct nontrivial models described by

$$H_{\vec{a}} = \vec{a} \cdot \vec{H}, \quad \vec{H} = (H_X, H_Y, H_Z) \quad (56)$$

with $\vec{a} = (\sin \theta \cos \varphi, \sin \theta \sin \varphi, \cos \theta)$. We can compose four exact scar eigenstates of this Hamiltonian, given by

$$|\Gamma_{\alpha\beta}^{\vec{a}}\rangle = \sum_{\vec{\sigma}} \vec{u}_\alpha^{a,\dagger} A^{s_1} \dots A^{s_{L_b}} \vec{u}_\beta^{\vec{a}} |\vec{s}\rangle, \quad (57)$$

$$\vec{u}_1^{\vec{a}} = \begin{pmatrix} \cos(\theta/2) \\ e^{i\varphi} \sin(\theta/2) \end{pmatrix}, \quad \vec{u}_2^{\vec{a}} = \begin{pmatrix} -e^{-i\varphi} \sin(\theta/2) \\ \cos(\theta/2) \end{pmatrix}. \quad (58)$$

The eigenvalue of $|\Gamma_{\alpha\beta}^{\vec{a}}\rangle$ is $\{(-1)^{\alpha-1} - (-1)^{\beta-1}\}/\sqrt{2}$. Using Eq. (33) and similar relations for the PXP model [9, 10] and the PZ₄P model [29] results in

$$\begin{aligned} H_{\vec{a}} |\Gamma_{\alpha\beta}^{\vec{a}}\rangle &= \sum_{\vec{\sigma}} \vec{u}_\alpha^{a,\dagger} (\vec{a} \cdot \vec{\Sigma}) A^{s_1} \dots A^{s_{L_b}} \vec{u}_\beta^{\vec{a}} |\vec{s}\rangle \\ &\quad - \sum_{\vec{\sigma}} \vec{u}_\alpha^{a,\dagger} A^{s_1} \dots A^{s_{L_b}} (\vec{a} \cdot \vec{\Sigma}) \vec{u}_\beta^{\vec{a}} |\vec{s}\rangle \end{aligned} \quad (59)$$

with $\vec{\Sigma} = (\sigma^x, \sigma^y, \sigma^z)/\sqrt{2}$, and then we confirm this by the fact that the vectors $\vec{u}_\alpha^{\vec{a}}$ are eigenvectors of $\vec{a} \cdot \vec{\Sigma}$ with eigenvalues $(-1)^{\alpha-1}/\sqrt{2}$.

Now, we are ready to construct a generalized version of the binary drive Eq. (35), represented by

$$H(t) = \vec{a}(t) \cdot \vec{H}, \quad \vec{a}(t+T) = \vec{a}(t). \quad (60)$$

Since $|\Gamma_{\alpha\beta}^{\vec{a}}\rangle$ is represented by a linear combination of $\{|\Gamma_{\alpha\beta}^x\rangle\}$ for arbitrary \vec{a} , the dynamics under $H(t)$ is closed within the subspace spanned by $\{|\Gamma_{\alpha\beta}^x\rangle\}$. Thus, this model always has a four-dimensional embedded subspace \mathcal{S} . Using the fact that $\{\vec{u}_\alpha^{\vec{a}}\}_{\alpha=1,2}$ is a complete orthonormal basis of \mathbb{C}^2 ,

$$|\Gamma_0\rangle \equiv |\Gamma_{11}^{\vec{a}}\rangle + |\Gamma_{22}^{\vec{a}}\rangle = \sum_{\vec{\sigma}} \text{Tr}[A^{s_1} \dots A^{s_{L_b}}] |\vec{s}\rangle, \quad (61)$$

which is independent of the choice of \vec{a} , is an eigenstate of $H_{\vec{a}}$ whose eigenvalue is 0. Thus, we always provide one of the four exact Floquet scar eigenstates of $H(t)$ with $|\Gamma_0\rangle$, whose quasienergy is 0.

VII. DISCUSSION AND CONCLUSIONS

Before concluding the paper, let us briefly discuss how to realize the Hamiltonian (35) showing Floquet quantum many-body scars. The PXP model, which hosts static quantum many-body scars, is experimentally realized in Rydberg atoms [4]. Each atom can occupy the ground state \downarrow and the Rydberg state \uparrow , which is an excited state with a large quantum number. Since the repulsive interactions between neighboring atoms in the Rydberg state are quite large, neighboring $\uparrow\uparrow$ pairs are prohibited. The Rabi oscillation in this limited subspace results in the PXP Hamiltonian H_X .

Once the PXP Hamiltonian H_X is realized, our model is also realizable. We consider a potential with quadruple periodicity of the lattice,

$$Z_4 = \sum_i c_i Z_i, \quad (62)$$

where the coefficients c_i are given by Eq. (14). Then, the Floquet operator U_f is

$$\begin{aligned} U_f &= e^{-iH_Y T_2} e^{-iH_X T_1} \\ &= e^{-i(-Z_4)(\pi/2)} e^{-iH_X T_2} e^{-iZ_4(\pi/2)} e^{-iH_X T_1}. \end{aligned} \quad (63)$$

Thus, our model can be realized by switching the PXP Hamiltonian and the quadruple-periodic potential alternately in the Rydberg atoms.

In summary, we have constructed a nonintegrable model which hosts Floquet quantum many-body scars, driven by uniformly-imposed Hamiltonians on the constrained Hilbert space prohibiting adjacent pairs of up spins. We have rigorously shown that the model violates Floquet-ETH with the fact that instantaneous Hamiltonians share a subspace immune to thermalization although the scar eigenstates do not correspond to one another. The entanglement spectrum of Floquet eigenstates and the real-time dynamics of the model indicate that any initial state outside of the embedded subspace is thermalized to infinite temperature. We have also discussed a possible experimental realization of the model in Rydberg atoms, and thereby our result would contribute to understanding how closed Floquet systems equilibrate to infinite temperature.

ACKNOWLEDGMENTS

This work is supported by a Grant-in-Aid for Scientific Research on Innovative Areas “Topological Materials Science” (KAKENHI Grant No. JP15H05855) and also JSPS KAKENHI (Grants No. JP16J05078, No. JP18H01140, and JP19H01838). K. M. is supported by Doctoral Program for World-leading Innovative & Smart Education, Ministry of Education, Culture, Sports, Science and Technology. K. T. thanks JSPS for support from Overseas Research Fellowship.

-
- [1] J. M. Deutsch, Phys. Rev. A **43**, 2046 (1991).
 - [2] M. Srednicki, Phys. Rev. E **50**, 888 (1994).
 - [3] M. Rigol, V. Dunjko, and M. Olshanii, Nature **452**, 854 (2008).
 - [4] H. Bernien, S. Schwartz, A. Keesling, H. Levine, A. Omran, H. Pichler, S. Choi, A. S. Zibrov, M. Endres, M. Greiner, V. Vuletić, and M. D. Lukin, Nature **551**, 579 (2017).
 - [5] N. Shiraishi and T. Mori, Phys. Rev. Lett. **119**, 030601 (2017).
 - [6] C. J. Turner, A. A. Michailidis, D. A. Abanin, M. Serbyn, and Z. Papić, Nature Physics **14**, 745 (2018).
 - [7] C. J. Turner, A. A. Michailidis, D. A. Abanin, M. Serbyn, and Z. Papić, Phys. Rev. B **98**, 155134 (2018).
 - [8] W. W. Ho, S. Choi, H. Pichler, and M. D. Lukin, Phys. Rev. Lett. **122**, 040603 (2019).
 - [9] N. Shiraishi, Journal of Statistical Mechanics: Theory and Experiment **2019**, 083103 (2019).
 - [10] C.-J. Lin and O. I. Motrunich, Phys. Rev. Lett. **122**, 173401 (2019).
 - [11] L. D’Alessio and M. Rigol, Phys. Rev. X **4**, 041048 (2014).
 - [12] A. Lazarides, A. Das, and R. Moessner, Phys. Rev. E **90**, 012110 (2014).
 - [13] H. C. Po, L. Fidkowski, T. Morimoto, A. C. Potter, and A. Vishwanath, Phys. Rev. X **6**, 041070 (2016).
 - [14] D. A. Abanin and Z. Papić, Annalen der Physik **529**, 1700169 (2017).
 - [15] D. V. Else, B. Bauer, and C. Nayak, Phys. Rev. Lett. **117**, 090402 (2016).
 - [16] C. W. von Keyserlingk, V. Khemani, and S. L. Sondhi, Phys. Rev. B **94**, 085112 (2016).
 - [17] V. Khemani, A. Lazarides, R. Moessner, and S. L. Sondhi, Phys. Rev. Lett. **116**, 250401 (2016).
 - [18] V. Khemani, C. W. von Keyserlingk, and S. L. Sondhi, Phys. Rev. B **96**, 115127 (2017).
 - [19] N. Y. Yao, A. C. Potter, I.-D. Potirniche, and A. Vishwanath, Phys. Rev. Lett. **118**, 030401 (2017).
 - [20] S. Choi, J. Choi, R. Landig, G. Kucsko, H. Zhou, J. Isoya, F. Jelezko, S. Onoda, H. Sumiya, V. Khemani, C. von Keyserlingk, N. Y. Yao, E. Demler, and M. D. Lukin, Nature **543**, 221 (2017).
 - [21] J. Zhang, P. W. Hess, A. Kyprianidis, P. Becker, A. Lee, J. Smith, G. Pagano, A. C. Potirniche, I.-D. and Potter, A. Vishwanath, N. Y. Yao, and C. Monroe, Nature **543**, 217 (2017).
 - [22] S. Pai and M. Pretko, Phys. Rev. Lett. **123**, 136401 (2019).
 - [23] V. Khemani and R. Nandkishore, arXiv:1904.04815 (2019).
 - [24] S. Sugiura, T. Kuwahara, and K. Saito, arXiv:1911.06092 (2019).
 - [25] See Section A2 in Appendix. We briefly review local observables and entanglement entropy of the infinite temperature state in the constrained Hilbert space.
 - [26] V. Khemani, C. R. Laumann, and A. Chandran, Phys.

- Rev. B **99**, 161101(R) (2019).
- [27] V. Oganesyan and D. A. Huse, Phys. Rev. B **75**, 155111 (2007).
 - [28] Y. Y. Atas, E. Bogomolny, O. Giraud, and G. Roux, Phys. Rev. Lett. **110**, 084101 (2013).
 - [29] See Section A1 in Appendix. This provides exact scar eigenstates of PZ₄P model and properties of the embedded subspace \mathcal{S} .
 - [30] T. Kuwahara, T. Mori, and K. Saito, Annals of Physics **367**, 96 (2016).
 - [31] T. Mori, T. Kuwahara, and K. Saito, Phys. Rev. Lett. **116**, 120401 (2016).
 - [32] D. A. Abanin, W. De Roeck, W. W. Ho, and F. Huveneers, Phys. Rev. B **95**, 014112 (2017).
 - [33] D. Abanin, W. De Roeck, W. W. Ho, and F. Huveneers, Commun. Math. Phys. **354**, 809 (2017).
 - [34] See Section A3 in Appendix. We demonstrate the real-time dynamics of special scar states under the Floquet drive.

Appendix

A1. PROPERTIES OF EMBEDDED SUBSPACE

A. Exact scar eigenstates of PZ₄P model

In this section, we show that the four matrix product states $|\Gamma_{\alpha\beta}^z\rangle$ ($\alpha, \beta = 1, 2$), given by

$$|\Gamma_{\alpha\beta}^z\rangle = \sum_{\vec{\sigma}} \vec{w}_\alpha^\dagger A^{s_1} \dots A^{s_{L_b}} \vec{w}_\beta |\vec{s}\rangle, \quad (\text{A1})$$

$$A^L = \begin{pmatrix} 0 & 0 \\ 0 & -\sqrt{2} \end{pmatrix}, \quad A^O = \begin{pmatrix} 0 & -1 \\ 1 & 0 \end{pmatrix}, \quad A^R = \begin{pmatrix} \sqrt{2} & 0 \\ 0 & 0 \end{pmatrix}, \quad \vec{w}_1 = \begin{pmatrix} 1 \\ 0 \end{pmatrix}, \quad \vec{w}_2 = \begin{pmatrix} 0 \\ 1 \end{pmatrix}, \quad (\text{A2})$$

are eigenstates of the PZ₄P Hamiltonian H_Z :

$$H_Z = \sum_{i=2}^{L-1} c_i P_{i-1} Q_i P_{i+1} + Q_1 P_2 + P_{L-1} Q_L, \quad (\text{A3})$$

$$c_i = \sqrt{2} \cos\left(\frac{i\pi}{2} - \frac{\pi}{4}\right), \quad Q_i = I_i - P_i = (1 + Z_i)/2. \quad (\text{A4})$$

Proof.—The proof goes in a similar way to the one for the PY₄P model in the main text. The terms acting on the b -th and $(b+1)$ -th blocks in H_Z , denoted by $h_{b,b+1}$, are given by

$$\begin{aligned} h_{b,b+1}^z &= (-1)^b (P_{2b-1} Q_{2b} P_{2b+1} + P_{2b} Q_{2b+1} P_{2b+2}) \\ &= (-1)^b (|R\rangle \langle R|)_b (I - |L\rangle \langle L|)_{b+1} + (-1)^b (I - |R\rangle \langle R|)_b (|L\rangle \langle L|)_{b+1} \\ &\equiv h_{b,b+1}^{z,(2)} + h_{b,b+1}^{z,(1)}, \end{aligned} \quad (\text{A5})$$

$$h_{b,b+1}^{z,(2)} = -2(-1)^b (|RL\rangle \langle RL|)_{b,b+1}, \quad h_{b,b+1}^{z,(1)} = (-1)^b (|R\rangle \langle R|)_b + (-1)^b (|L\rangle \langle L|)_{b+1}, \quad (\text{A6})$$

and the boundary terms are

$$Q_1 P_2 = (|L\rangle \langle L|)_1, \quad P_{L-1} Q_L = (|R\rangle \langle R|)_{L_b}. \quad (\text{A7})$$

The property $A^R A^L = O$ results in $h_{b,b+1}^{z,(2)} |\Gamma_{\alpha\beta}^z\rangle = 0$, and hence

$$H_Z |\Gamma_{\alpha\beta}^z\rangle = \sum_{b=1}^{L_b} h_b^{z,(1)} |\Gamma_{\alpha\beta}^z\rangle, \quad h_b^{z,(1)} = (-1)^b (|R\rangle \langle R| - |L\rangle \langle L|)_b \quad (\text{A8})$$

is obtained. When we move to the superblock picture, the action of $h_{2u-1}^{z,(1)} + h_{2u}^{z,(1)}$ can be calculated:

$$(h_{2u-1}^{z,(1)} + h_{2u}^{z,(1)}) |\Gamma_{\alpha\beta}^z\rangle = \sum_{\vec{t}} \vec{w}_\alpha^\dagger \tilde{A}^{t_1} \dots \tilde{G}^{t_u} \dots \tilde{A}^{t_{L_u}} \vec{w}_\beta |\vec{t}\rangle, \quad (\text{A9})$$

$$\tilde{G}^{(s,r)} = \left[\sum_{s'} (h_{2u-1}^{z,(1)})_{ss'} A^{s'} \right] A^r + A^s \left[\sum_{s'} (h_{2u}^{z,(1)})_{rr'} A^{r'} \right]. \quad (\text{A10})$$

By calculating \tilde{G}^t respectively for $t = (s, r)$, one can confirm the relation between \tilde{G}^t and \tilde{A}^t as

$$\tilde{G}^t = Z \tilde{A}^t - \tilde{A}^t Z, \quad t = OO, LL, RR, OL, OR, LO, RO, \quad (\text{A11})$$

where Z is defined by $Z = \sigma^z / \sqrt{2}$. Therefore, we obtain

$$H_Z |\Gamma_{\alpha\beta}^z\rangle = \sum_{\vec{t}} \vec{w}_\alpha^\dagger Z \tilde{A}^{t_1} \dots \tilde{A}^{t_{L_u}} \vec{w}_\beta |\vec{t}\rangle - \sum_{\vec{t}} \vec{w}_\alpha^\dagger \tilde{A}^{t_1} \dots \tilde{A}^{t_{L_u}} Z \vec{w}_\beta |\vec{t}\rangle \quad (\text{A12})$$

$$= \frac{1}{\sqrt{2}} \{(-1)^{\alpha-1} - (-1)^{\beta-1}\} |\Gamma_{\alpha\beta}^z\rangle, \quad (\text{A13})$$

and hence $|\Gamma_{\alpha\beta}^z\rangle$ are eigenstates of H_Z . \square

B. Relationship among PXP model, PY₄P model and PZ₄P model

We would like to note the relationship among the static models and explain how the PY₄P model and the PZ₄P model are constructed. First, let us introduce an embedded Hamiltonian, with which exact scar eigenstates can be systematically obtained [5]. An embedded Hamiltonian with an embedded subspace \mathcal{T} is given by

$$H_{\text{em}} = \sum_i P_i h_i P_i + H', \quad P_i \mathcal{T} = 0 \ (\forall i), \quad H' \mathcal{T} \subset \mathcal{T}, \quad (\text{A14})$$

where P_i is a projection operator. Although the nonintegrability is still nontrivial, the subspace \mathcal{T} is immune to thermalization since the dynamics under H_{em} is closed within it. It is known that the PXP Hamiltonian H_X can be transformed to a certain embedded Hamiltonian with the embedded subspace $\mathcal{S} = \text{span}\{|\Gamma_{11}^x\rangle, |\Gamma_{12}^x\rangle, |\Gamma_{21}^x\rangle, |\Gamma_{22}^x\rangle\}$ [9]. There are options of hermitian operators h_i and H' in Eq. (A14), as long as $P_i \mathcal{T} = 0$ and $H' \mathcal{T} \subset \mathcal{T}$ are satisfied. Ref. [9] claims that these options enable to construct generalized versions of the PXP Hamiltonian, which show exact quantum many-body scars. The PY₄P Hamiltonian H_Y , the PZ₄P Hamiltonian H_Z , and their linear combinations $\vec{a} \cdot \vec{H}$ exemplify the generalized versions, and we can find out them by imposing Rydberg blockade, which prohibits generation of adjacent up spins (i.e. PXP-type Hamiltonians), on the option of h_i and H' .

C. Observables

In this section, we calculate matrix elements of observables within the embedded subspace \mathcal{S} spanned by $\{|\Gamma_{\alpha\beta}^\nu\rangle\}_{\alpha,\beta=1,2}$. We consider a certain observable O_b acting on the b -th block, and then we define

$$F^s = \sum_{s'=O,L,R} (O_b)_{ss'} A^{s'}. \quad (\text{A15})$$

We can calculate the matrix elements $\langle \Gamma_{\alpha\beta}^\nu | O_b | \Gamma_{\alpha'\beta'}^\nu \rangle$ by

$$\begin{aligned} \langle \Gamma_{\alpha\beta}^\nu | O_b | \Gamma_{\alpha'\beta'}^\nu \rangle &= \sum_{\vec{s}} \{ (\vec{u}_\alpha^\nu)^\dagger A^{s_1} \dots A^{s_{L_b}} \vec{u}_\beta^\nu \}^* \{ (\vec{u}_{\alpha'}^\nu)^\dagger A^{s_1} \dots F^{s_b} \dots A^{s_{L_b}} \vec{u}_{\beta'}^\nu \} \\ &= (\vec{U}_{\alpha\alpha'}^\nu)^\dagger (E_{AA})^b E_{AF} (E_{AA})^{L_b-b-1} (\vec{U}_{\beta\beta'}^\nu), \end{aligned} \quad (\text{A16})$$

$$E_{AA} \equiv \sum_s (A^s)^* \otimes A^s = \begin{pmatrix} 2 & 0 & 0 & 1 \\ 0 & 0 & -1 & 0 \\ 0 & -1 & 0 & 0 \\ 1 & 0 & 0 & 2 \end{pmatrix}, \quad E_{AF} \equiv \sum_s (A^s)^* \otimes F^s, \quad \vec{U}_{\alpha\alpha'}^\nu \equiv (\vec{u}_\alpha^\nu)^* \otimes \vec{u}_{\alpha'}^\nu. \quad (\text{A17})$$

The norm and the overlap of $\{|\Gamma_{\alpha\beta}^\nu\rangle\}_{\alpha,\beta=1,2}$ are evaluated by setting $O_b = I_b$, which results in

$$\langle \Gamma_{11}^\nu | \Gamma_{11}^\nu \rangle = \langle \Gamma_{22}^\nu | \Gamma_{22}^\nu \rangle = \frac{1}{2}(3^{L_b} + 1), \quad \langle \Gamma_{12}^\nu | \Gamma_{12}^\nu \rangle = \langle \Gamma_{21}^\nu | \Gamma_{21}^\nu \rangle = \frac{1}{2}(3^{L_b} - 1), \quad (\text{A18})$$

$$\langle \Gamma_{11}^\nu | \Gamma_{12}^\nu \rangle = \langle \Gamma_{11}^\nu | \Gamma_{21}^\nu \rangle = \langle \Gamma_{22}^\nu | \Gamma_{12}^\nu \rangle = \langle \Gamma_{22}^\nu | \Gamma_{21}^\nu \rangle = \langle \Gamma_{12}^\nu | \Gamma_{21}^\nu \rangle = 0, \quad \langle \Gamma_{11}^\nu | \Gamma_{22}^\nu \rangle = 1 \quad (\text{A19})$$

for even L_b and $\nu = x, y, z$. Thus, under the renormalization by $|\tilde{\Gamma}_{\alpha\beta}^\nu\rangle \equiv |\Gamma_{\alpha\beta}^\nu\rangle / |||\Gamma_{\alpha\beta}^\nu\rangle||$, $\{|\tilde{\Gamma}_{\alpha\beta}^\nu\rangle\}_{\alpha,\beta=1,2}$ is an orthonormal basis of the embedded subspace \mathcal{S} .

Pauli x [z] operator for the b -th block are represented by $O_b = (|L\rangle\langle O| + |R\rangle\langle O| + \text{h.c.})_b$ [$O_b = -2(|O\rangle\langle O|)_b$] respectively. The matrix representation under the basis $\{|\tilde{\Gamma}_{\alpha\beta}^x\rangle\}_{\alpha,\beta=1,2}$ in the thermodynamic limit is given by the following equation:

$$\lim_{L \rightarrow \infty} \sum_{i=1}^L \langle \tilde{\Gamma}_{\alpha\beta}^x | X_i | \tilde{\Gamma}_{\alpha'\beta'}^x \rangle = \frac{1}{\sqrt{2}} \{ (-1)^{\alpha-1} - (-1)^{\beta-1} \} \delta_{\alpha\alpha'} \delta_{\beta\beta'}, \quad \lim_{L \rightarrow \infty} \frac{1}{L} \sum_{i=1}^L \langle \tilde{\Gamma}_{\alpha\beta}^x | Z_i | \tilde{\Gamma}_{\alpha'\beta'}^x \rangle = -\frac{1}{6} \delta_{\alpha\alpha'} \delta_{\beta\beta'}. \quad (\text{A20})$$

On the other hand, the domain wall density $D_b = (I_b - Z_{2b-1} Z_{2b})/2$ is obtained by setting $O_b = (|L\rangle\langle L| + |R\rangle\langle R|)_b$. The matrix representation under the basis $\{|\tilde{\Gamma}_{\alpha\beta}^\nu\rangle\}_{\alpha,\beta=1,2}$ in the thermodynamic limit is

$$\lim_{L_b \rightarrow \infty} \langle \tilde{\Gamma}_{\alpha\beta}^\nu | D_b | \tilde{\Gamma}_{\alpha'\beta'}^\nu \rangle = \frac{2}{3} \delta_{\alpha\alpha'} \delta_{\beta\beta'}, \quad \nu = x, y, z. \quad (\text{A21})$$

D. Floquet Intrinsic Scar Eigenstate

We discuss the relation between our model and *Floquet-intrinsic scar*, the exact Floquet quantum many-body scar recently proposed by S. Sugiura *et al.* [24]. They regard Floquet scar eigenstates which become simultaneous eigenstates of all the instantaneous frustration-free Hamiltonians $H(t)$ as trivial ones. In contrast to this, in the case of a binary drive Eq. (1), a Floquet-intrinsic scar eigenstate is defined by a scar eigenstate which is neither an eigenstate of H_1 nor that of H_2 , but a simultaneous eigenstate of their time evolution operators $\exp(-iH_1T_1)$ and $\exp(-iH_2T_2)$. Coexistence of these conditions is brought by the equivalence of quasienergy modulo 2π in Floquet systems, and hence Floquet-intrinsic scar eigenstates are unique to Floquet systems.

In our model, the Floquet eigenstate $|\Gamma_0\rangle$ is a simultaneous eigenstate of the instantaneous Hamiltonians H_X and H_Y . In general, the other three are neither an eigenstate of any instantaneous Hamiltonian nor that of its time evolution operator. Under fine-tuning of the parameters, Floquet-intrinsic scar eigenstates can appear in our model Eq. (35). Assume that the durations T_1 and T_2 are fixed as follows:

$$T_1 = \frac{(2m-1)\pi}{\sqrt{2}}, \quad T_2 = \frac{(2n-1)\pi}{\sqrt{2}}, \quad m, n \in \mathbb{N}. \quad (\text{A22})$$

Then, using Eq. (41), we find the four simultaneous eigenstates of $\exp(-iH_XT_1)$ and $\exp(-iH_YT_2)$. One is given by Eq. (44), and the other three $|\Gamma(u_X, u_Y)\rangle$ are as follows:

$$\begin{aligned} |\Gamma(+1, -1)\rangle &= |\Gamma_{11}^x\rangle - |\Gamma_{22}^x\rangle = i(|\Gamma_{12}^y\rangle - |\Gamma_{21}^y\rangle), \\ |\Gamma(-1, +1)\rangle &= |\Gamma_{12}^x\rangle - |\Gamma_{21}^x\rangle = i(|\Gamma_{11}^y\rangle - |\Gamma_{22}^y\rangle), \\ |\Gamma(-1, -1)\rangle &= |\Gamma_{12}^x\rangle + |\Gamma_{21}^x\rangle = |\Gamma_{12}^y\rangle + |\Gamma_{21}^y\rangle, \end{aligned} \quad (\text{A23})$$

where the indices $u_X, u_Y = \pm 1$ represent eigenvalues of $\exp(-iH_XT_1)$ and $\exp(-iH_YT_2)$ respectively. The state $|\Gamma(-1, -1)\rangle$, corresponding to the eigenstate Eq. (45), is neither an eigenstate of H_X nor that of H_Y , and it is a Floquet-intrinsic scar eigenstate. This Floquet-intrinsic scar eigenstate appears due to the emergent degeneracy of $|\Gamma_{12}^x\rangle$ and $|\Gamma_{21}^x\rangle$ under $\exp(-iH_XT_1)$ and that of $|\Gamma_{12}^y\rangle$ and $|\Gamma_{21}^y\rangle$ under $\exp(-iH_YT_2)$, although they are not originally degenerated under H_X or H_Y . This degeneracy is caused by equivalence of quasienergy modulo 2π unique to Floquet systems.

Floquet-intrinsic scar eigenstates are fragile to the change of parameters. In the originally-proposed model by S. Sugiura *et al.* [24], all the Floquet scar eigenstates found rigorously are Floquet-intrinsic scar eigenstates, and hence quantum many-body scars are not observed in the absence of fine-tuning. On the other hand, in our case, breakdown of the condition Eq. (A22) causes disappearance of the Floquet-intrinsic eigenstate as well, but the Floquet many-body scars still exist. In other words, our model includes Floquet-intrinsic scars as a special choice of the parameters.

A2. PROPERTIES OF INFINITE TEMPERATURE STATES

For this paper to be self-contained, we summarize the properties of the infinite temperature state in the constrained Hilbert space \mathcal{H} under Rydberg blockade [7]. We denote its dimension for the system size L under open boundary conditions by \mathcal{D}_L . The condition that pairs of adjacent up spins are prohibited results in

$$\mathcal{D}_1 = 2, \quad \mathcal{D}_2 = 3, \quad \mathcal{D}_{L+2} = \mathcal{D}_{L+1} + \mathcal{D}_L. \quad (\text{A24})$$

This is nothing but the definition of Fibonacci sequence, and hence we obtain

$$\mathcal{D}_L = \frac{1}{\sqrt{5}} \{ \phi^{L+2} - (1-\phi)^{L+2} \}, \quad \phi = \frac{1+\sqrt{5}}{2}. \quad (\text{A25})$$

A. Entanglement entropy

We evaluate the entanglement entropy at infinite temperature when we split the system in half. Denoting the left half (the right half) by A (B), the reduced density operator of the infinite temperature state $\rho_\infty = I_{\mathcal{D}_L}/\mathcal{D}_L$ for the subsystem A is

$$\rho_\infty^A \equiv \text{Tr}_B[\rho_\infty] = \frac{1}{\mathcal{D}_L} \left(\mathcal{D}_{L/2-1} \sum_{\vec{\sigma} \in \mathcal{K}_\uparrow} |\vec{\sigma}\rangle \langle \vec{\sigma}| + \mathcal{D}_{L/2} \sum_{\vec{\sigma} \in \mathcal{K}_\downarrow} |\vec{\sigma}\rangle \langle \vec{\sigma}| \right). \quad (\text{A26})$$

Here, we define \mathcal{K}_\uparrow (\mathcal{K}_\downarrow) by a set of configurations of $L/2$ spins, whose spin at the right edge is \uparrow (\downarrow). Using the equations $|\mathcal{K}_\uparrow| = \mathcal{D}_{L/2-2}$ and $|\mathcal{K}_\downarrow| = \mathcal{D}_{L/2-1}$, we obtain the entanglement entropy at infinite temperature as follows:

$$S_\infty \equiv -\text{Tr}_A[\rho_\infty^A \log \rho_\infty^A] = -\frac{\mathcal{D}_{L/2-2}\mathcal{D}_{L/2-1}}{\mathcal{D}_L} \log\left(\frac{\mathcal{D}_{L/2-1}}{\mathcal{D}_L}\right) - \frac{\mathcal{D}_{L/2-2}\mathcal{D}_{L/2-1}}{\mathcal{D}_L} \log\left(\frac{\mathcal{D}_{L/2-2}}{\mathcal{D}_L}\right), \quad (\text{A27})$$

and in the thermodynamic limit, the entanglement entropy per volume becomes

$$\lim_{L \rightarrow \infty} \frac{S_\infty}{L} = \frac{1}{2} \log \phi. \quad (\text{A28})$$

B. Observables

The expectation value of a certain observable O at infinite temperature is given by

$$\langle O \rangle_{T=\infty} \equiv \frac{1}{\mathcal{D}_L} \text{Tr}_{\mathcal{H}}[O] = \frac{1}{\mathcal{D}_L} \sum_{\vec{\sigma} \in \mathcal{K}_L} \langle \vec{\sigma} | O | \vec{\sigma} \rangle, \quad (\text{A29})$$

where \mathcal{K}_L represents a set of classical spin configurations of an L -site chain which includes no adjacent up spins.

We here discuss the expectation values of the Pauli operators X_i , Z_i , and the domain wall density D_b . Since the operator X_i has only off-diagonal elements in the basis $\{|\vec{\sigma}\rangle\}_{\vec{\sigma} \in \mathcal{K}_L}$, we obtain

$$\langle X_i \rangle_{T=\infty} = \frac{1}{\mathcal{D}_L} \sum_{\vec{\sigma} \in \mathcal{K}_L} \langle \vec{\sigma} | X_i | \vec{\sigma} \rangle = 0. \quad (\text{A30})$$

Next, we consider the Pauli z operator Z_i . When we fix the i -th spin by \uparrow (\downarrow), the number of possible spin configurations is $\mathcal{D}_{i-2} \times \mathcal{D}_{L-i-1}$ ($\mathcal{D}_{i-1} \times \mathcal{D}_{L-i}$). Therefore, we obtain the expectation value for finite-size and infinite-size systems as follows:

$$\langle Z_i \rangle_{T=\infty} = \frac{1}{\mathcal{D}_L} \sum_{\vec{\sigma} \in \mathcal{K}_L} \langle \vec{\sigma} | Z_i | \vec{\sigma} \rangle = \frac{\mathcal{D}_{i-2}\mathcal{D}_{L-i-1} - \mathcal{D}_{i-1}\mathcal{D}_{L-i}}{\mathcal{D}_L}, \quad \lim_{L \rightarrow \infty} \langle Z_i \rangle_{T=\infty} = -\frac{1}{\sqrt{5}}. \quad (\text{A31})$$

In a similar way, we obtain the domain wall density as follows:

$$\langle D_b \rangle_{T=\infty} = \frac{1}{\mathcal{D}_L} \sum_{\vec{\sigma} \in \mathcal{K}_L} \langle \vec{\sigma} | D_b | \vec{\sigma} \rangle = \frac{\mathcal{D}_{2b-3}\mathcal{D}_{2L_b-2b} + \mathcal{D}_{2b-2}\mathcal{D}_{2L_b-2b-1}}{\mathcal{D}_{2L_b}}, \quad \lim_{L_b \rightarrow \infty} \langle D_b \rangle_{T=\infty} = \frac{2}{\sqrt{5}\phi}. \quad (\text{A32})$$

A3. DYNAMICS OF SPECIAL SCAR STATES

In this section, we discuss the relationship between the model showing exact Floquet many-body scars and a non-thermalizing oscillation of observables in the static PXP model [4, 6]. In the PXP model, the embedded subspace spanned by the exact scar eigenstates is perfectly immune to thermalization. However, there also exist some special scar states seemingly immune to thermalization although they are not included in the embedded subspace. In fact, an extremely long-term oscillation of the domain wall density is observed under the preparation of special initial states such as $|\mathbb{Z}_2\rangle = |\uparrow\downarrow\uparrow\downarrow\dots\rangle$ and $|\mathbb{Z}_3\rangle = |\uparrow\downarrow\downarrow\uparrow\downarrow\dots\rangle$ in Rydberg atoms. Our periodically-driven model is composed of the PXP Hamiltonian H_X and the PY₄P Hamiltonian H_Y , and each of them shows non-thermalizing oscillations of observables under the specific initial-state preparation (See Fig. A1 (a) for the non-thermal behavior of the PY₄P model). Here, we numerically examine whether a non-thermalizing oscillation appears also in the driven cases, and discuss its origin.

Figure A1 shows the real-time dynamics when we begin with the \mathbb{Z}_2 ordered state $|\mathbb{Z}_2\rangle$ [See (b) and (c)]. Figure A1 (c) indicates that the model for the relatively-small period $T = T_1 + T_2 = 1$ shows non-thermalizing oscillations of the domain wall density $D_{L/2}$ and the Pauli operator $Z_{L/2}$. These non-thermalizing behaviors are expected to originate from pre-equilibration of Floquet systems in the high-frequency regime [30–33]. When the local energy scale of the Hamiltonian is small enough compared to the frequency, its stroboscopic dynamics is well described by a static effective Hamiltonian given by the Floquet-Magnus expansion. Up to the lowest order in T , the static effective Hamiltonian for our model is given by the time-averaged one over one period,

$$H_{\text{eff}} = \frac{T_1}{T_1 + T_2} H_X + \frac{T_2}{T_1 + T_2} H_Y + O(T). \quad (\text{A33})$$

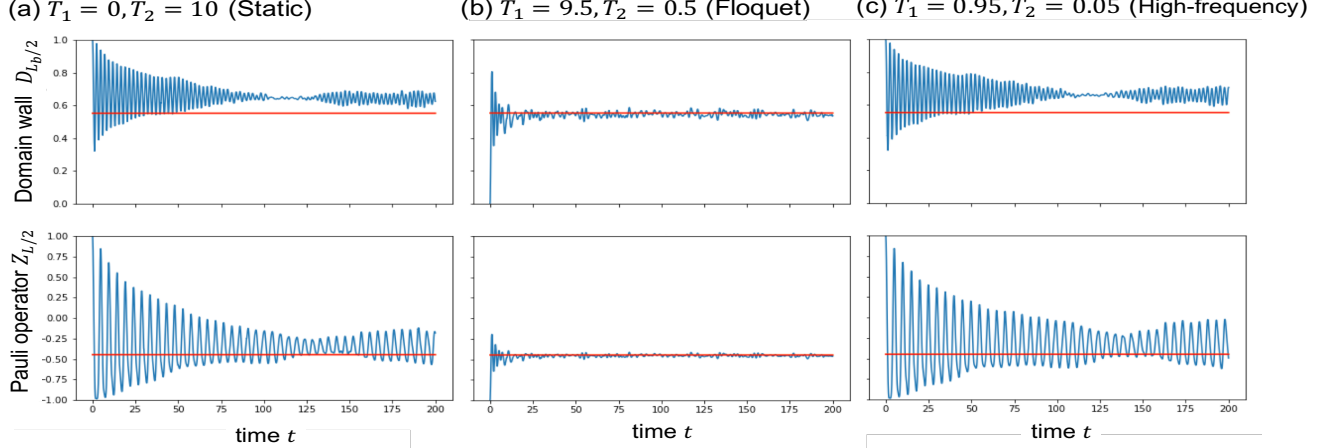


FIG. A1. Real-time dynamics under the special initial state $|\mathbb{Z}_2\rangle = |\uparrow\downarrow\uparrow\downarrow\dots\rangle$: (a) under the static PY_4P Hamiltonian (b) under the binary drive at $T_1 = 9.5, T_2 = 0.5$ (c) under the binary drive at $T_1 = 0.95, T_2 = 0.05$. (a) Both of the domain wall density and the Pauli z operator show long-lasting oscillations without approaching their thermal equilibrium values at $T = \infty$. (b) The observables rapidly approach those of the infinite temperature due to the drive. (c) Non-thermalizing behaviors of the observables are observed as in the static case in spite of the existence of the drive. These are brought by pre-equilibration under an effective static Hamiltonian in the high-frequency regime of Floquet systems.

Thus, through Fig. A1 (c), we observe non-thermalizing behaviors caused by static quantum many-body scars in the periodically-driven model.

On the other hand, when the local energy scale is comparable to the frequency or larger than it, we expect that effective static behaviors do not appear. Figure A1 (b) shows the dynamics for such a Floquet intrinsic regime, where the local energy scale 1 is larger than the frequency $2\pi/T = \pi/5$. This result represents that the domain wall density $D_{L/2}$ and the Pauli operator $Z_{L/2}$ quickly relax to the values of infinite temperature states, and that the non-thermalizing oscillations disappear by the periodic drive in spite of the instantaneous Hamiltonians H_X and H_Y . We focus on the origin of this behavior below.

We expect that this can be explained in terms of forward scattering approximation (FSA) [6, 7]. By means of FSA, we can obtain an approximately-closed subspace of the dynamics under a certain initial state, and write down the effective Hamiltonian within this subspace. In the case of the PXP model, the Hamiltonian H_X can be divided into two terms as follows:

$$H_X = H_X^+ + H_X^-, \quad H_X^+ = \sum_{i:\text{odd}} P_{i-1} S_i^- P_{i+1} + \sum_{i:\text{even}} P_{i-1} S_i^+ P_{i+1}, \quad H_X^- = (H_X^+)^\dagger, \quad (\text{A34})$$

$$S_i^\pm = \frac{1}{2}(X_i \pm iY_i), \quad P_0 = P_{L+1} = I \quad (\text{A35})$$

under open boundary conditions. When we begin with $|\mathbb{Z}_2\rangle$, we define a set of orthonormal states by

$$|v_0\rangle = |\mathbb{Z}_2\rangle, \quad |v_n\rangle = \frac{(H_X^+)^n |v_0\rangle}{\|(H_X^+)^n |v_0\rangle\|}, \quad n = 0, 1, 2, \dots, L. \quad (\text{A36})$$

When we denote the Hamming distance (the smallest number of spin flips required to convert two states each other) from $|\mathbb{Z}_2\rangle$ by $H.D.$, the term H_X^+ (H_X^-) increases (decreases) $H.D.$ by one. Thus, the state $|v_n\rangle$ becomes a superposition of states whose spin configurations satisfy $H.D. = n$, and thereby we obtain $|v_L\rangle = |\tilde{\mathbb{Z}}_2\rangle$ and $|v_{L+1}\rangle = 0$. From the numerical calculation up to $L = 32$ [7], it is known that the dynamics from the initial state $|\mathbb{Z}_2\rangle$ under H_X is approximately closed within the subspace \mathcal{R}_X , spanned by $\{|v_n\rangle\}_{n=0}^L$ [See Fig. A2 (a)]. This is one of the possible explanations for long-term non-thermalizing oscillations in the PXP model [6, 7].

In a similar way, we apply FSA to the PY_4P model. The Hamiltonian is written as

$$H_Y = H_Y^+ + H_Y^-, \quad H_Y^+ = -i \sum_{i:\text{odd}} c_i P_{i-1} S_i^- P_{i+1} + i \sum_{i:\text{even}} c_i P_{i-1} S_i^+ P_{i+1}, \quad H_Y^- = (H_Y^+)^\dagger, \quad (\text{A37})$$

(a) PXP model

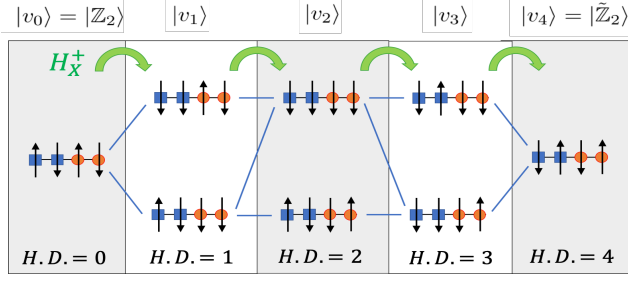
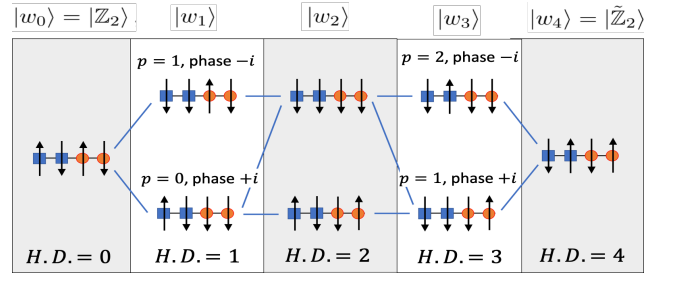
(b) PY₄P model

FIG. A2. Schematic pictures of approximately-closed subspaces obtained by FSA: (a) for the PXP model and (b) for the PY₄P model at $L = 4$. Blue squares and orange circles represent $c_i = +1$ and $c_i = -1$ at their positions respectively. Each layer denoted by $|v_n\rangle$ or $|w_n\rangle$ is composed of product states whose Hamming distance from $|\mathbb{Z}_2\rangle$ is fixed to n . In the PY₄P model, phase differences between states in the same layer appear depending on c_i , as depicted in the figure (b) as “phase”.

and then the dynamics under H_Y is approximately closed within the subspace \mathcal{R}_Y spanned by $\{|w_n\rangle = (H_Y^+)^n |\mathbb{Z}_2\rangle / \|(H_Y^+)^n |\mathbb{Z}_2\rangle\| \}_{n=0}^L$. A state $|w_n\rangle$ is a superposition of states whose Hamming distance from $|\mathbb{Z}_2\rangle$ is n as well, but each state in it has an additional phase represented by

$$(-i)^{\sum_{i:\text{odd}} c_i Q_i} \times i^{\sum_{i:\text{even}} c_i P_i}. \quad (\text{A38})$$

This is schematically depicted in Fig. A2 (b). Then, we can understand the thermalization to infinite temperature under the Floquet drive with the initial state $|\mathbb{Z}_2\rangle$ from the difference between the closed subspaces \mathcal{R}_X and \mathcal{R}_Y . We immediately obtain $|v_0\rangle = |w_0\rangle$, $|v_L\rangle = |w_L\rangle$, and $\langle v_i | w_j \rangle = 0$ for different i, j by their definitions. First, let us consider the overlap between $|v_1\rangle$ and $|w_1\rangle$. These states are equally-weighted superpositions of states with $H.D. = 1$, and each state in the latter one has an additional phase $+i$ or $-i$ depending on c_i of the flipped site. Thus, we obtain

$$\langle v_1 | w_1 \rangle = \frac{1}{N_{H.D.=1}} \{ (-i) \times L/4 + i \times L/4 \} = 0, \quad (\text{A39})$$

where $N_{H.D.=n}$ represents the number of possible spin configurations with $H.D. = n$ under the constrained Hilbert space. Next, we consider the overlap $\langle v_n | w_n \rangle$ for generic n in the limit of $L \rightarrow \infty$. Here, let p denote the number of flipped spins with $c_i = +1$ required to obtain from $|\mathbb{Z}_2\rangle$ [See Fig. A2 (b) for example]. Then, each state in $|w_n\rangle$ has an additional phase given by $(+i)^p (-i)^{n-p} = (-1)^p (-i)^n$, and the overlap $\langle v_n | w_n \rangle$ is determined by its summation over states with $H.D. = n$. Let us consider the case where n is odd. The additional phase $(-1)^p (-i)^n$ depends on the parity of p . Choosing odd p flipped sites with $c_i = +1$ is equivalent to choosing even $n - p$ flipped sites with $c_i = -1$. Assume that the system size L is large enough, and then we can neglect the effect of the boundaries. With considering the symmetry of $c_i = +1$ and $c_i = -1$ in the bulk, the total number of states with odd p is equal to that for even p . Thus, we obtain

$$\lim_{L \rightarrow \infty} \langle v_n | w_n \rangle = 0, \quad \text{for odd } n \quad (\text{A40})$$

because $N_{H.D.=n}$ grows with increasing L . These macroscopic number (at least $L/2$) of orthogonality relations represent that a generic state in \mathcal{R}_X (or \mathcal{R}_Y) flows out of \mathcal{R}_X (or \mathcal{R}_Y) under the time evolution by the Hamiltonian H_Y (or H_X). Finally, we conclude that, under the periodic switching of H_X and H_Y , the dynamics from $|\mathbb{Z}_2\rangle$ is no longer closed within the original subspaces \mathcal{R}_X or \mathcal{R}_Y , and hence thermalization to infinite temperature is observed without showing non-thermalizing oscillations.